Journal of Sound and Vibration (1999) **221**(1), 143–167
Article No. jsvi.1998.1987, available online at http://www.idealibrary.com.on IDEAL

RADIATION DAMPING IN PLATES, INDUCED BY POROUS MEDIA†

A. CUMMINGS

School of Engineering, University of Hull, Hull HU6 7RX, U.K.

H. J. RICE

Department of Mechanical and Manufacturing Engineering, Trinity College Dublin, Dublin, Ireland

AND

R. WILSON

School of the Built Environment, University of Nottingham, Nottingham NG7 2RD, U.K.

(*Received* 17 *February* 1998, *and in final form* 2 *October* 1998)

Experimental data on the damping properties of a simply supported aluminium plate mounted in a rigid baffle, and separated by an air gap from a slab of open-celled plastic foam, are presented along with numerical results from two independent analyses. The first is a coupled modal analysis incorporating a finite-thickness layer of absorbent and a baffle of finite dimensions. The second is a plate radiation model with an infinite baffle and an absorbent of semi-infinite extent. Numerical predictions from the two models and the experimental data are generally in reasonable agreement, and the roles of both the plate/absorbent spacing and the mode of vibration of the plate are highlighted. It is shown, for example, that the loss factor of the plate is very strongly dependent on the air space and that the damping varies quite markedly between different plate modes. The damping is also strongly dependent on the steady flow resistivity of the porous medium. Predictions of the power dissipation per unit volume in the absorbent (with no air gap) and of the intensity distribution over the plate surface (with an air gap) illustrate some interesting features of the behaviour of the system.

1. INTRODUCTION

The transverse vibration of a thin metal plate, mounted with low-loss boundary conditions, is normally lightly damped if the plate radiates into a gas. Acoustic radiation, internal losses and dissipation at the boundaries are the prevailing damping mechanisms, but the combined effect of these is nonetheless fairly small. If, however, a layer of porous, acoustically dissipative material is placed near the

† A shorter version of this paper was presented at the ISMA21 Conference in Leuven, Belgium, 18–20 September 1996.

0022–460X/99/110143 + 25 $30.00/0

surface of the plate then a resistive near-field is created, and "gas-pumping" effects within the absorbent bring about very substantial energy losses by viscous and thermal mechanisms. The increase in structural loss factor can be very high and depends on the spacing between the plate and the surface of the absorbent, and on the bulk acoustic properties of the absorbent. This plate damping problem contains some of the essential features of the damping mechanisms prevailing in sound transmission through aircraft fuselages—in which a porous thermal insulation blanket is situated within the double-panel structure between the outer skin and the interior trim panel—and also in lightweight double-wall building partitions. A related problem has been investigated by Astley *et al*. [1], who found that an internal lining of porous material, placed adjacent to a flexible duct wall, brought about very large axial attenuation of ductborne sound around the lowest transverse wall resonance frequency. The physical mechanism is similar to that in the plate vibration problem considered here, although attention was not focused, in reference [1], on the wall damping, but rather on sound attenuation in the duct. A fairly obvious question arises in this context, concerning whether the porous medium should be considered flexible, or whether an equivalent fluid representation would be adequate in theoretical modelling. In reference [1], good agreement between prediction and measurement was obtained by the use of an equivalent fluid formulation but it should be noted that, in the experimental tests carried out in that investigation, there was little or no contact between the solid frame of the absorbent and the duct wall. Bolton *et al*. [2] have fairly recently reported a study of sound transmission through multiple panels containing elastic porous blankets, and one of their concluding remarks is of particular interest here: "If the foam layer is separated from the panel by an airspace, relatively well-damped airborne waves are better excited in the lining than the lightly damped frame and shear waves." This suggests that, provided there is no solid contact between the vibrating plate and the absorbent layer, an equivalent fluid representation of the absorbent (in which frame flexibility is not taken into account) might be adequate. Panneton and Atalla [3] came to a similar conclusion in a numerical study of sound transmission through double-wall structures with poroelastic blankets between the panels but also added, "... the mixed configuration, bonded–unbonded, is preferred to the bonded or unbonded configuration." Evidently—as might be expected—a poroelastic medium, bonded to a panel, exerts a greater damping effect than it would if it were not bonded (because of enhanced structural coupling between the panel and the solid frame of the material, and vibrational damping losses in the frame), thereby increasing the transmission loss of the double-wall structure. Equally, the solid frame of the absorbent, if bonded to both panels, can act as a vibration bridge between the panels, thus lowering the transmission loss. Allard [4] has presented analyses of structures involving plates and porous layers, though he did not address himself explicitly to the question of the effects of the porous material on the plate damping.

In this paper, we report the results from a study of the effects of a layer of porous material placed a distance away from a simply supported plate which is mounted in a baffle and vibrating in one of its normal modes. Experimental results for the plate loss factor are given and two independent theoretical analyses are described

and used to provide numerical data for comparison. Because of the nature of the experimental apparatus, neither theoretical model alone could be expected to yield accurate predictions for all the modes considered. On the other hand, both models taken together do provide a complete coverage and comparisons between all three sets of data give a valuable insight into the mechanisms responsible for radiation damping. The parametric dependence of loss factor on separation distance and flow resistivity of the absorbent—for a commonly used material—is also presented, and this illustrates the range of structural damping that is achievable. The computed distribution of energy dissipation per unit volume in the absorbent and intensity distribution over the plate surface are shown for typical cases, and help to illustrate the physical mechanisms of damping.

2. MEASUREMENTS

An experimental investigation of sound radiation into a porous medium was conducted by using the baffled aluminium plate and slab of plastic foam shown in the upper part of Figure 1. An electrodynamic shaker, connected to the plate *via* a force transducer, was used to excite the system and mobility spectra were obtained from the frequency response function between the applied force signal and the velocity measured at a number of points on the plate. A modal curve fitting procedure was employed to determine the damping of the plate from the modal peaks in the mobility spectra. From these data it was possible to infer the contribution to the total damping resulting from radiation from the plate into the porous layer.

2.1. MEASUREMENT ARRANGEMENT AND ABSORBENT PROPERTIES

A 1-mm thick aluminium plate measuring 458×250 mm was used in the experiments. These dimensions were selected to provide a fundamental frequency of about 50 Hz (close to the first mode in a typical aircraft fuselage bay) and as wide a modal separation as possible, to facilitate the experimental identification of structural modes. The baffle was constructed from a 43-mm thick sheet of plywood to provide a substantial structural discontinuity and hence weak coupling between itself and the plate. An approximation to a simply supported boundary condition was obtained by using the technique illustrated in the lower part of Figure 1. Sharp pins were glued into grooves cut at 15 mm centres in a 1·5-mm thick aluminium strip and this was then fixed around the perimeter of the aperture in the baffle. The pins were then forced up against the edges of the plate firmly enough to secure it in place but not so firmly as to cause buckling. This left a 1·5-mm wide gap around the plate perimeter, which was sealed with a strip of thin aluminium tape to prevent acoustic leakage between the air on opposite sides of the baffle. An M6 nut was glued to the plate and used to secure the force transducer, which was then connected to the shaker *via* a slender rod (or "moment arrester"); this arrangement is shown in Figure 2. White noise was fed to the shaker to excite the system.

A $1{\cdot}45 \times 1{\cdot}24 \times 0{\cdot}345$ m slab of partially reticulated combustion modified polyether foam was used as the porous medium. This material had a bulk density

of 39 kg/m^3 and a steady flow resistivity, σ, of 6992 mks rayl/m. Foam was used in preference to (say) glass fibre blanket because its relatively isotropic properties simplified the theoretical analysis. Although any anisotropy in the bulk properties of the foam used in the present experiments was not examined in detail, experience has shown that most polyether and polyester foams may be treated as effectively isotropic for most practical purposes. A further advantage of using foam was its relative ease in handling and positioning. The bulk acoustic properties of the foam (which is treated here as an equivalent fluid) were measured by using an impedance tube technique, over the frequency range 63 Hz–2 kHz. The acoustic characteristic

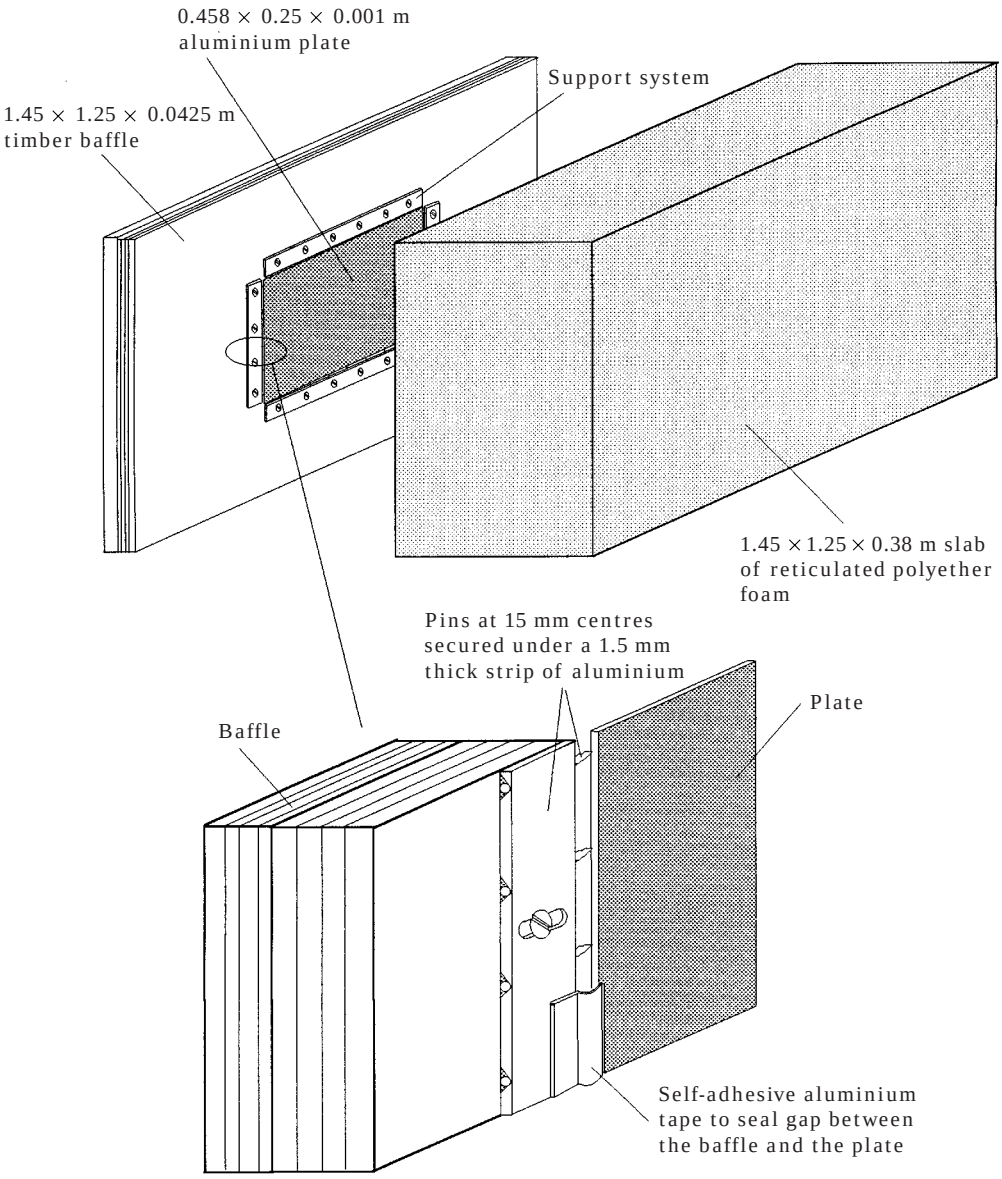

Figure 1. System for mounting the plate in a baffle; (x, y) dimensions: plate—a, b; baffle—L_a, L_b.

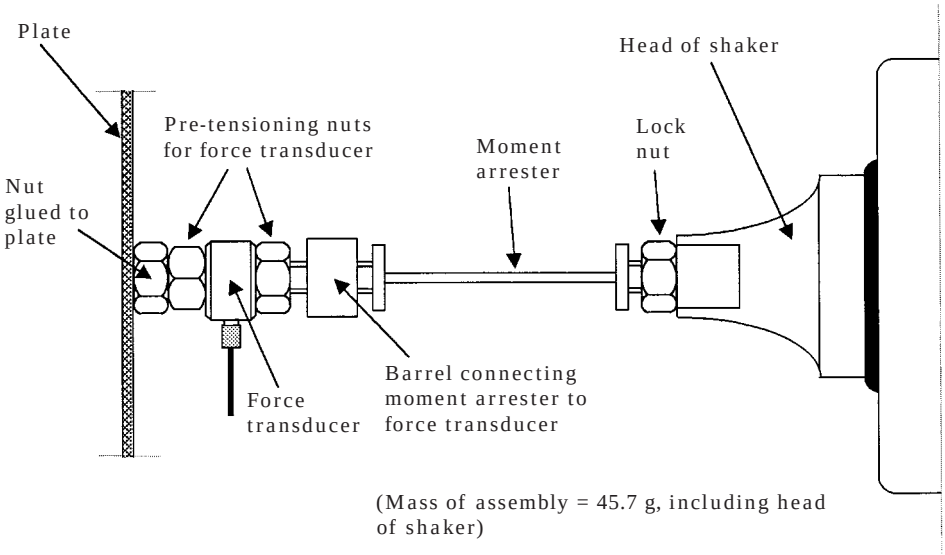

Figure 2. The method of fixing the shaker to the plate.

impedance Z_a and propagation coefficient Γ_a at frequency f were represented in the following form, ρ being the air density, c the sound speed and k the acoustic wavenumber:

$$Z_a/\rho c = 1 + c_1\xi^{c_2} - \mathrm{i}c_3\xi^{c_4} \quad \text{and} \quad \Gamma_a/k = c_5\xi^{c_6} + \mathrm{i}(1 + c_7\xi^{c_8}). \qquad (1a, b)$$

Here ξ is the dimensionless frequency given by

$$\xi = \rho f/\sigma. \qquad (2)$$

The coefficients $c_1 - c_8$ were found from regression lines through the measured data, which yielded $c_1 = 0{\cdot}1590$, $c_2 = -0{\cdot}5517$, $c_3 = 0{\cdot}0632$, $c_4 = -0{\cdot}8730$, $c_5 = 0{\cdot}1442$, $c_6 = -0{\cdot}7323$, $c_7 = 0{\cdot}2779$, $c_8 = -0{\cdot}3699$. This follows the approach used by Delany and Bazley [5], although their curve-fitting formulae give incorrect results if they are used to extrapolate the measured data below the lower end of their frequency range ($\xi \approx 0{\cdot}012$, corresponding to $f = 70$ Hz for the foam used here). In order to avoid this problem, the low frequency model of Kirby and Cummings [6] was employed for predictive purposes in the two theoretical formulations described in this paper. This involves the use of the Delany and Bazley formulae with coefficients as given above, together with a parallel-fibre model of the absorbent and an empirically-determined, real, frequency-dependent tortuosity and shape factor. Low frequency approximations to Bessel and Neumann functions are used, but these are valid from zero frequency to frequencies well above the range of interest here. The low frequency model is a way of extrapolating measured data (i.e., the real and imaginary parts of both Z_a and Γ_a) to arbitrarily low frequencies while retaining physically reasonable values of tortuosity and pore shape factor, and at the same time predicting the correct limiting values of the bulk acoustic parameters as $\xi \to 0$.

2.2. MEASUREMENT PROCEDURE AND DATA ANALYSIS

Mobility measurements were initially performed with the plate radiating into air on both sides. As a means of providing a check on the vibrational mode shapes of the plate, measurements of the approximate mode shapes were performed in the absence of the porous layer at a series of points arranged in a grid over the plate surface. The frequency response function between the velocity at these points (measured by the use of a roving accelerometer) and the force measured at the driving point was taken, and the mode shapes were determined from the magnitude and phase of this function at frequencies where the mobility plots exhibited peaks (see section 5 of this paper). The foam slab was then introduced and measurements were performed with air gaps of 1·6, 4·5, 7·3, 10·2, 13, 15·9, 18·7, 38, 57 and 114 mm. For each air gap the frequency response function between the acceleration measured at a range of locations on the plate surface and the excitation force was recorded. This was then converted into mobility by dividing the data by $i\omega$ (ω = radian frequency).

A robust experimental modal analysis (see the paper by Xu [7]) of the measured mobility spectra was performed, yielding the total loss factor of the plate modes, comprising the boundary losses, internal losses and losses from sound radiation into the surrounding fluid. For the case where the fluid is air, the radiation losses are usually insignificant and the total loss factor is dominated by the losses at the plate boundary. When, however, a porous material is introduced on one side of the plate, there will be an increase in the radiated sound power and a corresponding rise in the total loss factor. This new radiation loss can be extracted by subtracting the total loss factor, for the plate radiating into air, from the total loss factor for the plate radiating into the porous material, and adding to this the theoretical loss factor for the plate radiating into air from both sides.

3. A MODAL FORMULATION

The experimental baffled plate system may be modelled as three finite domains, as shown in section in Figure 3. The radiation loss on the upper surface of the absorbent may be modelled by assuming the existence of an infinitely long duct with finite rectangular cross-section ($L_a \times L_b$). The "duct walls" are assumed to impose a pressure release boundary condition, and this same boundary condition is assumed also to prevail at the perimeters of the absorbent layer and the air space. This choice of boundary condition is convenient in the present case in that it renders the analysis relatively straightforward as compared to cases involving other possible boundary conditions. The radiation effects (assumed to be slight) on the underside of the plate will not be modelled directly in this analysis but will be taken in account by the imposition of experimentally observed structural damping and stiffness parameters on the overall system in the tuning and verification process described below. The dynamics of the overall system may now be formulated by coupling of the individual subsystem equations.

3.1. STRUCTURAL SYSTEM (PLATE)

The transverse response of the plate $w(x\,y;\omega)$ may be expressed in terms of its uncoupled mode shapes as

$$w = \sum_{i=1}^{n_s} \phi_{i_s}(x, y) q_{i_s}(\omega), \tag{3}$$

where w is the complex amplitude of upward displacement of the plate at a particular frequency ω, q_{i_s} is the response of the ith structural mode ϕ_{i_s} and n_s is the number of modes used in the expansion. Equation (3) can be expressed in vector form as

$$w = \mathbf{\Phi}_s \mathbf{q}_s, \tag{4}$$

where $\mathbf{\Phi}_s$ is a row vector of the structural mode shapes and $\mathbf{q}_s$ is a column vector of the modal responses. For the simply supported case and for the dimensions shown, the plate equation will be satisfied by mass normalized mode shapes given as

$$\phi_{s_i} = (2/\sqrt{M_p}) \sin[(x + a/2 - L_a/2)m_i\pi x/a] \sin[(y + b/2 - L_b/2)n_i\pi y/b], \tag{5}$$

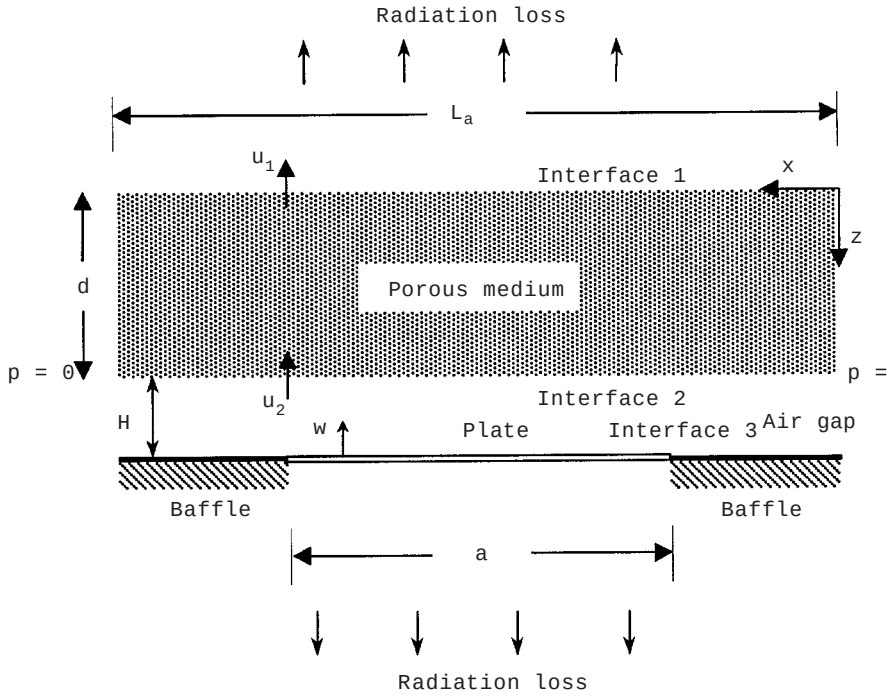

Figure 3. The plate, air space and absorbent system.

where M_p is the mass of the plate, a, b are its transverse dimensions and m_i, n_i are the x, y mode numbers associated with the ith mode. The natural frequencies of the modes will be given by

$$\omega_{s_i}^2 = [\pi^4 E t^2/12\rho_p(1-\nu^2)](m_i^2/a^2 + n_i^2/b^2)^2, \tag{6}$$

where E, ν, t, ρ_p are the Young's modulus, Poisson's ratio, thickness and material density of the plate, respectively, although in this analysis the experimentally observed values of plate frequencies are substituted for theoretical values in the verification of the modal formulation. If the plate is loaded by a point force f at a position (x_l, y_l) and is loaded on the fluid side by a pressure distribution $p_f(x, y; \omega)$, then the response of the ith structural mode is given by

$$(-\omega^2 + \mathrm{i}2\zeta_{s_i}\omega_{s_i}\omega + \omega_{s_i}^2)q_{s_i} = -\int_{(L_a-a)/2}^{(L_a+a)/2}\int_{(L_b-b)/2}^{(L_b+b)/2} p_f\phi_{s_i}\,\mathrm{d}y\,\mathrm{d}x + f\phi_{s_i}(x_l, y_l), \tag{7}$$

ζ_{s_i} being the damping ratio of the ith plate mode.

3.2. AIR GAP MODEL

Upon assuming that the acoustic pressure within the air gap does not vary significantly with height, one can also expand the pressure in terms of n_f of its uncoupled mode shapes as

$$p_f(x, y; \omega) = \Phi_f(x, y)q_f(\omega), \tag{8}$$

where the normalized mode shapes are given by

$$\phi_{f_i} = (2c/\sqrt{L_a L_b H})\sin(m_i\pi x/L_a)\sin(n_i\pi y/L_b), \tag{9}$$

H being the width of the air space between the plate and the absorbent. Imposing the Helmholtz equation then yields the associated natural frequencies, which are given by

$$\omega_{f_i}^2 = \pi^2 c^2(m_i^2/L_a^2 + n_i^2/L_b^2). \tag{10}$$

The acoustical loading in this section of the model is generated by the interfacial flow $u_2(x, y; \omega)$ and the plate motion w.

The fluid modal response is therefore governed by

$$(-\omega^2 + \omega_{f_i}^2)q_{f_i} = -\mathrm{i}\omega\rho\int_0^{L_a}\int_0^{L_b} u_2\phi_{f_i}\,\mathrm{d}y\,\mathrm{d}x - \rho\omega^2\int_{(L_a-a)/2}^{(L_a+a)/2}\int_{(L_b-b)/2}^{(L_b+b)/2} w\phi_{f_i}\,\mathrm{d}y\,\mathrm{d}x. \tag{11}$$

3.3. ABSORBENT SYSTEM MODEL

To complete the system model, an expression for the interfacial fluid velocity u_2 in equation (11) must be determined from a model of the absorbent sub-system. In the equivalent fluid model, it is assumed that the absorbent may be completely characterized by its characteristic impedance Z_a and its porosity Γ_a, and when

harmonically excited it then assumes an equivalent sound speed and density given by

$$c_a = \mathrm{i}\omega/\Gamma_a, \qquad \rho_a = Z_a\Gamma_a/\mathrm{i}\omega. \tag{12, 13}$$

The acoustic pressure within the porous medium $p_a(x, y, z;\ \omega)$ can then be assumed to obey the equivalent Helmholtz equation

$$\nabla^2 p_a + (\omega^2/c_a^2)p_a = 0. \tag{14}$$

In order to satisfy the various boundary conditions it is convenient to separate the x, y and z variables according to

$$p_a = F(x, y; \omega)G(z; \omega), \tag{15}$$

which yields the equations

$$\partial^2 G/\partial z^2 + \lambda_a^2 G = 0, \qquad \nabla^2 F + (\omega^2/c_a^2 - \lambda_a^2)F = 0. \tag{16, 17}$$

Equation (17), together with its boundary conditions, is satisfied and pressure compatibility at interface 2 is assured by the solution

$$p_a(d) = \sum_{i=1}^{n_f} q_{f_i}\phi_{f_i}G_i(d), \qquad G_i(d) = 1, \tag{18, 19}$$

$$\lambda_{ai}^2 = \omega^2/c_a^2 - m_i^2\pi^2/L_a^2 - n_i^2\pi^2/L_b^2, \tag{20}$$

where d is the absorbent thickness in the z direction. A solution of equation (16) which obeys (19) is

$$G_i = [(1 - A_i \sin \lambda_i d)/\cos \lambda_i d] \cos \lambda_i z + A_i \sin \lambda_i z, \tag{21}$$

where A_i is a constant which is determined by the boundary condition on the upper surface of the absorbent. This constant is fixed by developing an expression for the interfacial fluid velocity u_1 from equation (15),

$$u_1 = (1/\mathrm{i}\omega\rho_a)F\,\partial G(0)/\partial z. \tag{22}$$

Expressing this in terms of an impedance,

$$u_1 = (1/\mathrm{i}\omega\rho_a)\{[\partial G(0)/\partial z]/G(0)\}p_a(x, y, 0; \omega), \tag{23}$$

allows a comparison to be made with the impedance of an infinite duct to a propagating wave having a cross-sectional sound pressure distribution given by ϕ_{f_i}. This impedance is given by

$$Z_{2_i} = \rho\omega/\lambda_i, \tag{24}$$

where

$$\lambda_i = \sqrt{\omega^2/c^2 - m_i^2\pi^2/L_a^2 - n_i^2\pi^2/L_b^2}. \tag{25}$$

Hence

$$\rho\omega/\lambda_i = -(1/\mathrm{i}\omega\rho_a)A_i\lambda_{a_i} \cos \lambda_{a_i}/(1 - A_i \sin \lambda_{a_i}), \tag{26}$$

which gives a solution for G_i as

$$G_i = \frac{\sin \lambda_{a_i} z - \mathrm{i}(\rho\lambda_{a_i}/\rho_a\lambda_i)\cos \lambda_{a_i} z}{\sin \lambda_{a_i} d - \mathrm{i}(\rho\lambda_{a_i}/\rho_a\lambda_i)\cos \lambda_{a_i} d}. \tag{27}$$

Finally, from equations (22) and (18) one arrives at an expression for u_2,

$$u_2 = \sum_{i=1}^{n_f} \frac{\lambda_{a_i}}{\mathrm{i}\omega\rho_a}\left[\frac{\cos \lambda_{a_i} d + \mathrm{i}(\rho\lambda_{a_i}/\rho_a\lambda_i)\sin \lambda_{a_i} d}{\sin \lambda_{a_i} d - \mathrm{i}(\rho\lambda_{a_i}/\rho_a\lambda_i)\cos \lambda_{a_i} d}\right]\phi_{f_i} q_{f_i}. \tag{28}$$

3.4. ASSEMBLY OF SYSTEM MODEL

When expression (8) for p_f is substituted into equation (7), one may write

$$(-\omega^2\mathbf{I} + \mathrm{i}\omega\mathbf{D} + \Omega_s^2)\mathbf{q}_s + \mathbf{S}^{\mathrm{T}}\mathbf{q}_f = \mathbf{f}, \tag{29}$$

where the coupling matrix $\mathbf{S}$ is given by

$$\mathbf{S} = \int_{(L_a-a)/2}^{(L_a+a)/2} \int_{(L_b-b)/2}^{(L_b+b)/2} \boldsymbol{\Phi}_f^{\mathrm{T}} \boldsymbol{\Phi}_s \, \mathrm{d}y \, \mathrm{d}x \tag{30}$$

and the diagonal structural damping and stiffness matrices are given by

$$D_{ii} = 2\zeta_i \omega_{s_i} \quad \text{and} \quad \Omega_{s_{ii}}^2 = \omega_{s_i}^2. \tag{31, 32}$$

The forcing vector $\mathbf{f}$ is given by

$$\mathbf{f} = f\boldsymbol{\Phi}_s^{\mathrm{T}}(x_l, y_l). \tag{33}$$

Similarly, the fluid model in equation (11), with an additional substitution for u_2 according to equation (28), may be expressed as

$$-\rho\omega^2\mathbf{S}\mathbf{q}_s + (-\omega^2\mathbf{I} + \mathrm{i}\omega\mathbf{R} + \Omega_f^2)\mathbf{q}_f = \mathbf{0}, \tag{34}$$

where the fluid damping caused by the absorbent is modelled by the $\mathbf{R}$ matrix as

$$R_{ij} = \int_0^{L_a} \int_0^{L_b} \mathrm{Re}\left\{\frac{\rho\lambda_{a_j}}{\mathrm{i}\omega\rho_a}\left[\frac{\cos \lambda_{a_j} d + \mathrm{i}(\rho\lambda_{a_j}/\rho_a\lambda_j)\sin \lambda_{a_j} d}{\sin \lambda_{a_j} d - \mathrm{i}(\rho\lambda_{a_j}/\rho_a\lambda_j)\cos \lambda_{a_j} d}\right]\right\}\phi_{f_j}\phi_{f_i} \, \mathrm{d}y \, \mathrm{d}x. \tag{35}$$

Because of the orthogonality of the fluid mode shapes over the integration interval in (35), $\mathbf{R}$ is diagonal with entries given by

$$R_{ii} = \mathrm{Re}\left\{\frac{c^2\rho\lambda_{a_i}}{H\mathrm{i}\omega\rho_a}\left[\frac{\cos \lambda_{a_i} d + \mathrm{i}\rho\lambda_{a_i}/\rho_a\lambda_i \sin \lambda_{a_i} d}{\sin \lambda_{a_i} d - \mathrm{i}\rho\lambda_{a_i}/\rho_a\lambda_i \cos \lambda_{a_i} d}\right]\right\}. \tag{36}$$

Relationship (28) will also give rise to an imaginary component, which can be considered as a fluid stiffness. Hence,

$$\Omega_{f_{ii}}^2 = \omega_{f_i}^2 - \frac{1}{\omega}\,\mathrm{Im}\left\{\frac{c^2\rho\lambda_{a_i}}{H\mathrm{i}\omega\rho_a}\left[\frac{\cos \lambda_{a_i} d + \mathrm{i}(\rho\lambda_{a_i}/\rho_a\lambda_i)\sin \lambda_{a_i} d}{\sin \lambda_{a_i} d - \mathrm{i}(\rho\lambda_{a_i}/\rho_a\lambda_i)\cos \lambda_{a_i} d}\right]\right\}. \tag{37}$$

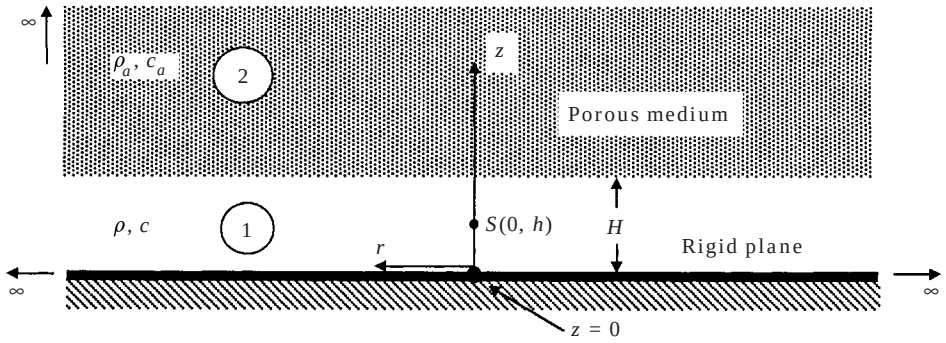

Figure 4. A monopole located in the air space between a rigid plane and an absorbent.

Equations (29) and (34) may now be solved directly for $\mathbf{q}_s$ and hence a frequency response function at a chosen response point (x_r, y_r), according to

$$\Xi(x_r, y_r, x_l, y_l; \omega) = \mathbf{\Phi}_s(x_r, y_r)\mathbf{q}_s/f. \tag{38}$$

The equivalent modal damping and natural frequencies may now be derived from the frequency response $\Xi(\omega)$ by using a curve fitting procedure such as that described at Xu [7]. Although it is conceivable that these parameters could also be found by examining the eigenvalues of a homogenous system of equations formed from equations (29) and (34), the curve fitting approach facilitates a more direct comparison with supporting experiments.

4. A RADIATION MODEL FOR PLATE DAMPING

Here, an alternative model is described for the radiation damping of a simply supported, baffled plate that is separated from a semi-infinite layer of dissipative, porous acoustic medium (represented as an equivalent fluid), by a layer of the fluid contained in the pores of the medium. The other side of the plate radiates into a semi-infinite region of the same fluid. The method of calculation of the sound power dissipated per unit volume in the absorbent is also outlined, in the case where there is no air space between the panel and the absorbent. The assumption of infinite lateral dimensions for the absorbent and air gap is implicit in the radiation model chosen here; to impose finite lateral dimensions with prescribed boundary conditions would complicate the analysis considerably. However, this feature helps to differentiate the present analysis from the modal formulation of section 3, thereby facilitating comparisons between two fundamentally different models (see sections 5 and 6).

4.1. THE SOUND FIELD ON A RIGID PLANE, FROM A POINT SOURCE

Consider an acoustic monopole S, of volume strength S_0, located a distance h above a rigid plane, in the space (medium 1, fluid density ρ and sound speed c) between the plane and a semi-infinite layer of absorbing material (medium 2,

effective density ρ_a and sound speed c_a; see Figure 4). One may express the sound field in region 1 as

$$p(r, z; t) = (\mathrm{i}\omega\rho S_0/4\pi)\exp(\mathrm{i}\omega t)P_1(r, z) \tag{39}$$

and take the formulation of Ewing *et al*. [8] (see also the paper by Amédin *et al*. [9]), with acoustic pressure as the scalar field variable, to give

$$P_1(r, z) = \int_0^\infty \frac{\kappa}{v_1} \mathrm{J}_0(\kappa r)\,\mathrm{e}^{-v_1|z-h|}\,\mathrm{d}\kappa + \int_0^\infty Q_{11}(\kappa)\mathrm{J}_0(\kappa r)\,\mathrm{e}^{-v_1(z-h)}\,\mathrm{d}\kappa$$

$$+ \int_0^\infty Q_{12}(\kappa)\mathrm{J}_0(\kappa r)\,\mathrm{e}^{v_1(z-h)}\,\mathrm{d}\kappa \tag{40a}$$

and

$$P_2(r, z) = \int_0^\infty Q_2(\kappa)\mathrm{J}_0(\kappa r)\,\mathrm{e}^{-v_2(z-h)}\,\mathrm{d}\kappa, \tag{40b}$$

where $P_2(r, z)$ is the spatial factor in region 2. The Q functions are determined from the boundary conditions and $v_1 = \sqrt{\kappa^2 - k^2}$, $v_2 = \sqrt{\kappa^2 - k_a^2}$, k_a being the complex, effective wavenumber in medium 2. Application of the rigid-wall boundary condition at $z = 0$ and continuity of sound pressure and particle velocity at $z = H$ yields expressions for the Q functions, and hence an integral expression for $P_1(r, 0)$, the spatial factor for the sound pressure at the plate surface with $h = 0$. The integrand is singular at $\kappa = k$, but this singularity may be removed by transforming the variable of integration from κ to v_1; the integration path is then along the imaginary axis from ik to 0, then along the real axis to ∞. A further transformation leads to the following result (α being a real variable):

$$P_1(r, 0) = 2\int_0^k \frac{\sqrt{k^2 - k_a^2 - \alpha^2}\sin\alpha H + \delta\alpha\cos\alpha H}{\sqrt{k^2 - k_a^2 - \alpha^2}\cos\alpha H - \delta\alpha\sin\alpha H}\mathrm{J}_0(r\sqrt{k^2 - \alpha^2})\,\mathrm{d}\alpha$$

$$+2\int_0^\infty \frac{\sqrt{k^2 - k_a^2 + \alpha^2}\sinh\alpha H + \delta\alpha\cosh\alpha H}{\sqrt{k^2 - k_a^2 + \alpha^2}\cosh\alpha H + \delta\alpha\sinh\alpha H}\mathrm{J}_0(r\sqrt{k^2 + \alpha^2})\,\mathrm{d}\alpha, \tag{41}$$

δ being the complex ratio of the effective fluid density in the porous medium to the real fluid density. The first integral can be evaluated numerically without too much difficulty by the use of Gauss–Legendre quadrature (with an appropriate number of sub-intervals), but the second is less easy, since it converges slowly and is infinite. In this case, Gauss–Legendre quadrature was again employed, with adjustable sub-intervals. To obtain reasonable accuracy, 12-point quadrature was used, with 1000 sub-intervals.

4.2. THE SOUND POWER RADIATED BY ONE SIDE OF THE PLATE

It is customary to find the sound power radiated by a vibrating structure from the acoustic far field, but this cannot be done in the present case because sound power flow is not conserved between the plate surface and the far field. A different strategy must therefore be adopted. The sound pressure at point $O(x, y)$ on the surface of the plate (see Figure 5), radiated by a source element at $S(x_s, y_s)$ is

$$\delta p(x, y|x_s, y_s; t) = \left(\frac{i\omega\rho}{4\pi}\right) e^{i\omega t}\, \dot{W}_0 \delta x_s \delta y_s \sin\left(\frac{m\pi x_s}{a}\right) \sin\left(\frac{n\pi y_s}{b}\right) P_1(r, 0), \quad (42)$$

where

$$r = [(x - x_s)^2 + (y - y_s)^2]^{1/2} \quad (43)$$

and $\dot{W}_0$ is the amplitude of the vibrational velocity $\dot{w}$ of the plate. The total sound pressure at $O(x, y)$, from the entire plate, is therefore

$$p(x, y; t) = \Sigma \delta p(x, y|x_s, y_s; t)$$

$$= \frac{i\omega\rho\, e^{i\omega t}\dot{W}_0}{4\pi} \int_0^b \int_0^a \sin\left(\frac{m\pi x_s}{a}\right) \sin\left(\frac{n\pi y_s}{b}\right) P_1(r, 0)\, dx_s\, dy_s. \quad (44)$$

The normal component of the radiated acoustic intensity $I_z(x, y)$ at the surface of the plate is given by

$$I_z(x, y) = \overline{\mathrm{Re}\,[p(x, y; t)\, \mathrm{Re}\,[\dot{w}(x, y; t)]}$$

$$= -\frac{\omega\rho\dot{W}_0^2}{8\pi} \sin\left(\frac{m\pi x}{a}\right) \sin\left(\frac{n\pi y}{b}\right) \int_0^b \int_0^a \sin\left(\frac{m\pi x_s}{a}\right) \sin\left(\frac{n\pi y_s}{b}\right)$$

$$\times \mathrm{Im}\,[P_1(r, 0)]\, dx_s\, dy_s, \quad (45)$$

and integrating this over the plate area yields the total radiated sound power,

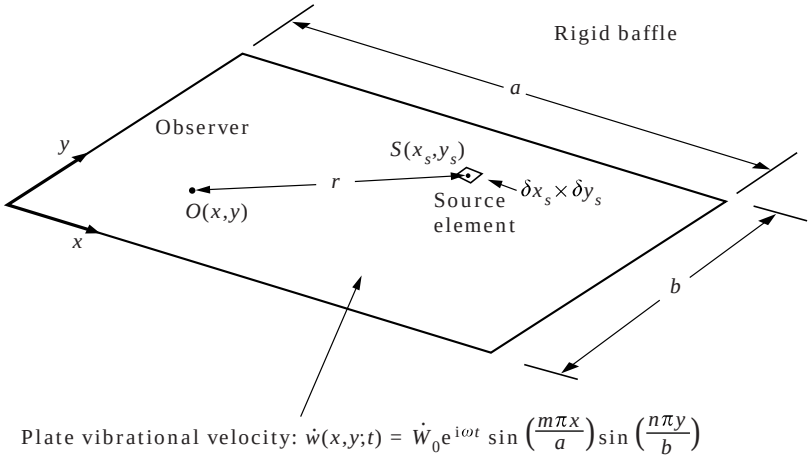

Figure 5. Geometry of the plate.

$$W_{rad} = -\frac{\omega\rho\dot{W}_0^2}{8\pi}\int_0^b\int_0^a \sin\left(\frac{m\pi x}{a}\right)\sin\left(\frac{n\pi y}{b}\right)\int_0^b\int_0^a \sin\left(\frac{m\pi x_s}{a}\right)\sin\left(\frac{n\pi y_s}{b}\right)$$

$$\times \operatorname{Im}\left[P_1(r, 0)\right] \mathrm{d}x_s\, \mathrm{d}y_s\, \mathrm{d}x\, \mathrm{d}y. \tag{46}$$

This integration apparently cannot be carried out analytically, and so Gauss–Legendre quadrature was employed, piecewise over each "phase cell" of the plate vibration pattern. In order to avoid singularities in the computation at points where $x = x_s$ and $y = y_s$, six-point quadrature was used for the inner two integrals and five-point quadrature for the outer two. The sound power radiated from one side of the plate can be found from equation (46). The computation was carried out twice, once for the plate radiating into the absorbent and once for radiation into air (i.e., from the reverse side of the plate), and the two sound power values were added together to yield the total radiated power from both sides of the plate. The figures obtained for the plate radiating into air were compared to data published by Wallace [10], and very close correspondence was noted.

4.3. THE LOSS FACTOR OF RESONANT PLATE MODES

It may readily be shown from elementary considerations that the effective loss factor η for the (m, n) mode of a plate simply supported along all its edges is related to W_{rad} by the expression

$$\eta = 1{\cdot}273 W_{rad}/f_{mn} M_p \dot{W}_0^2, \tag{47}$$

where f_{mn} is the undamped modal natural frequency. The theoretical undamped plate frequencies were used in carrying out the computations based on the radiation model. Equation (47) gives predictions that are consistent with those derived from the experimental data by the use of the modal analysis method [7], albeit at slightly different frequencies for a given plate mode, depending on the degree of damping. These small frequency differences are of little consequence in the present context.

4.4. SOUND POWER DISSIPATED PER UNIT VOLUME IN THE ABSORBENT

The sound pressure dissipated per unit volume in the absorbent may be found from the sound pressure field as follows. The acoustic intensity vector may be expressed as

$$\mathbf{I}(x, y) = \overline{\operatorname{Re}\left[p(x, y; t)\right] \operatorname{Re}\left[\mathbf{v}(x, y; t)\right]}, \tag{48}$$

where $\mathbf{v}$ is the particle velocity vector. In a steady state, in a dissipative medium, the balance of acoustic energy requires that

$$w_{diss} + \nabla \cdot \mathbf{I} = 0, \tag{49}$$

where w_{diss} is the time averaged rate of dissipation of acoustic energy per unit volume in the medium. For sinusoidal time variation, equation (48) may also be expressed

$$\mathbf{I} = \tfrac{1}{2} \operatorname{Re}\left(P^*\mathbf{V}\right), \tag{50}$$

where P and $\mathbf{V}$ are the amplitudes of sound pressure and particle velocity, respectively. From the linearized Euler equation

$$\mathbf{V} = -\nabla P/\mathrm{i}\omega\rho_a, \tag{51}$$

and so equation (49) yields

$$w_{diss} = -(1/2\omega)\,\mathrm{Re}\,[\mathrm{i}(P^*\nabla^2 P + \nabla P \cdot \nabla P^*)/\rho_a]. \tag{52}$$

From the Helmholtz equation for the porous medium,

$$\nabla^2 P = -k_a^2 P \tag{53}$$

and one can show that

$$w_{diss} = -\{\rho_{ai}\nabla P \cdot \nabla P^* - [\rho_{ai}(k_{ar}^2 - k_{ai}^2) - 2\rho_{ar}k_{ar}k_{ai}]|P|^2\}/2\omega|\rho_a|^2, \tag{54}$$

where $\rho_a = \rho_{ar} + \mathrm{i}\rho_{ai}$ and $k_a = k_{ar} + \mathrm{i}k_{ai}$. From equation (54), one can readily find w_{diss} from the sound pressure field.

For the sake of simplicity, the sound pressure field was determined in the absence of an air space; the results would also be valid for a very small air space. The sound field was determined from the radiation model by integrating the plate velocity over the surface of the plate as in equation (44), with the spatial factor $P_1(r, 0)$ replaced by $2(\rho_a/\rho)\exp(-\mathrm{i}k_a R)/R$, R being the distance from the point (x_s, y_s) on the plate to the field point, equal to $[(x - x_s^2)^2 + (y - y_s^2)^2 + z^2]^{1/2}$. In this case 12-point Gauss–Legendre quadrature was employed, over each phase cell on the plate, so that the gradients of P and P^* in equation (54) could be found to the required accuracy by the use of a finite-difference approximation.

5. RESULTS

A selection of experimental mobility functions is shown in Figure 6. As the porous material is introduced and moved closer to the plate, two phenomena may be observed: the modal frequency drops, because of the effective additional attached mass of the air in the foam and air gap, and the damping increases as a result of increased acoustic radiation.

The measured mode shapes for the five lowest plate modes, with the plate radiating into air on both sides (see section 2.2), are shown in Figure 7. These correspond well to the theoretical mode shapes. The mobility peak at about 132 Hz in Figure 6 appears to be "spurious" in that it does not correspond to one of the normal modes for a simply supported plate, but may well be associated with the excitation system; it is not shown in Figure 7.

Predicted and measured values of the plate radiation loss factor η—for the test plate—versus air gap width H are shown in Figure 8(a), for the (1, 1) mode, with an undamped natural frequency of 51·7 Hz, and the (2, 1) mode, with a frequency of 87·3 Hz. Numerical predictions from both the modal formulation and the radiation model are shown. It may be noted that the latter model predicts a constant value of η for $H \to 0$, a broad maximum in η at $H \approx 1{\cdot}5$ mm and a monotonic decrease in η as $H \to \infty$ (η actually tends asymptotically to the air radiation value). For the (1, 1) mode, the modal formulation predicts the loss

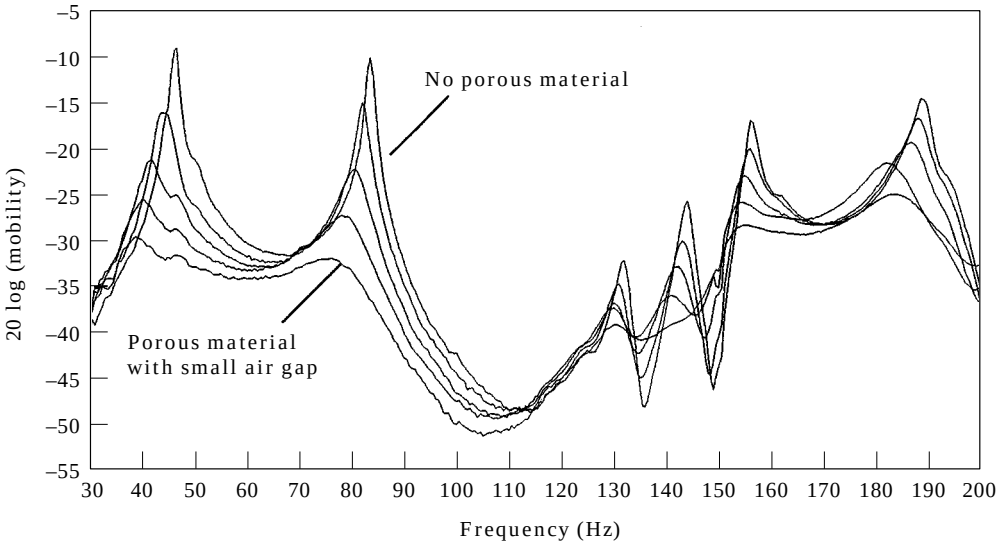

Figure 6. Measured mobility spectra for a variety of air gap widths.

factor fairly well (with an overestimate, particularly for $H > 6$ mm), whereas the radiation model forecasts figures which are significantly too high overall. This might be expected, since the finite absorbent thickness is taken into account in the modal formulation, but in the radiation model the absorbent is assumed to be infinitely thick, leading to an overestimate of the acoustic losses. The assumption of infinite lateral dimensions for the absorbent and air gap—in the radiation model—doubtless has its effects on the predictions too, though these are thought likely to be smaller than those associated with the absorbent thickness. In the case of the (2, 1) mode, the radiation model predicts η to quite good accuracy, but the modal formulation is in rather poor agreement with experiment, both qualitatively and quantitatively. The reasons for this are not entirely clear, but may be associated at least partly with the assumed boundary conditions at the perimeter of the layer of absorbent and with the (duct) model for radiation from the absorbent layer. That the radiation model should perform better in this case might be expected since, at this higher frequency (and with greater propagation losses in the absorbent), the assumption of an infinite absorbent thickness should be less restrictive than it is in the case of the (1, 1) mode. In Figure 8(b) the measured loss factor and that predicted from the radiation model are shown, for the (3, 1) and (2, 2) modes. Agreement between prediction and measurement is good. Since the (3, 1) mode is a net volume-displacing mode whereas the (2, 2) mode is not, its radiation loss factor in air alone is substantially higher (despite its lower natural frequency), and is shown on the plot. One can see that, for $H = 0{\cdot}1$ m, the loss factor of panel plus absorbent is only about twice that of the panel in air alone.

It is of interest to investigate the details of both the acoustic intensity on the surface of the test plate and the spatial distribution of the sound power dissipation within the porous absorbent. The intensity is given by equation (45), and the double integration was carried out numerically by using five-point Gauss–Legendre quadrature piecewise over each phase cell. Contours of the intensity distribution—computed from the radiation model—over one phase cell of the (2, 2) mode (one-quarter of the plate), for $\dot{W}_0 = 1$ m/s, are shown in Figure 9. Figure 9(a) shows the results for the plate radiating into air and Figure 9(b) shows the results for the plate radiating into the absorbent, with $H = 5$ mm. This mode is, at its natural frequency, a "corner mode" and the intensity distribution in Figure 9(a) reflects this, being concentrated in the lower left-hand corner of the phase cell shown; the radiated intensity is appropriately small. By contrast, in Figure 9(b), it may be seen that the presence of the absorbent transforms the mode into something equivalent to a "surface mode", not by wavelength matching effects but by the introduction of local near-field dissipative effects. The radiation is now concentrated around the centre of the phase cell, indicating a much more evenly distributed radiation resistance, and the intensity values are now very much greater.

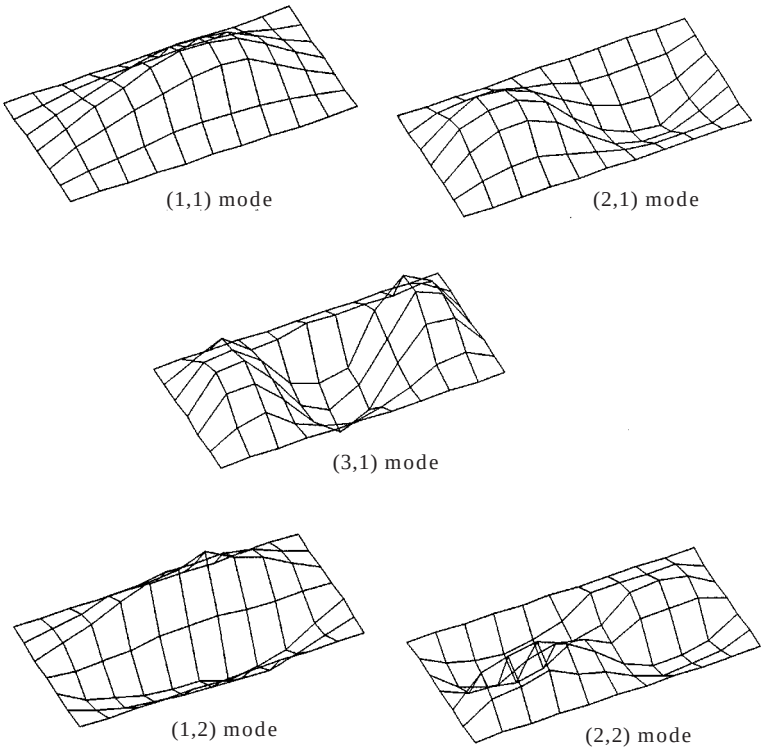

Figure 7. Mode shapes for the lowest plate modes.

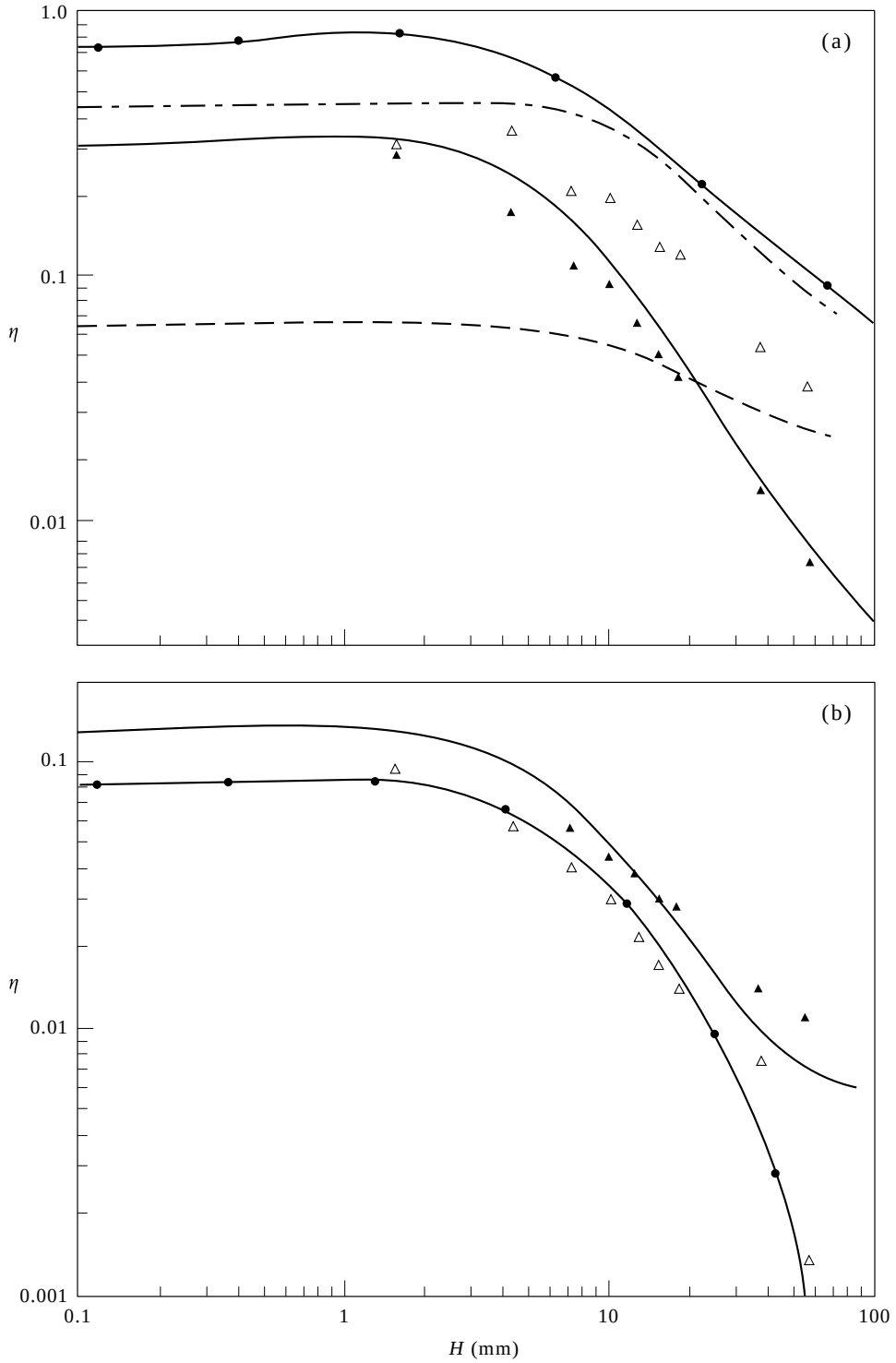

Figure 8. Measured and predicted loss factors. (a) △, ●——●, — – —: measured, radiation model, modal formulation for the (1, 1) mode; ▲, ———, – – –: measured, radiation model, modal formulation for the (2, 1) mode. (b) ▲, ———: measured, radiation model for the (3, 1) mode; △, ●——●: measured, radiation model for the (2, 2) mode.

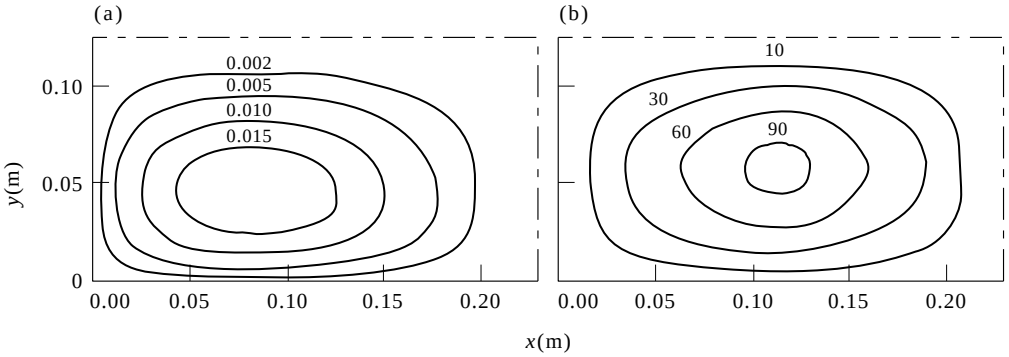

Figure 9. Predicted intensity contours on the plate surface for a phase cell from the (2, 2) mode: (a) plate radiating into air, (b) plate radiating into absorbent, $H = 5$ mm; contour values are W/m^2.

The sound power dissipation, per unit volume, in the absorbent, was found as described in section 4.4. In Figure 10, contours of w_{diss} in the absorbent are shown for the test plate vibrating in the (1, 1) and (1, 2) plate modes, in the yz plane at $x = 0{\cdot}229$ m, for $H = 0$. Again, $\dot{W}_0 = 1$ m/s. It can be seen from Figure 10(a) that, for the (1, 1) mode, w_{diss} falls off by a factor of ten within about 0·2 m and by a factor of 500 within about 0·5 m. The power dissipation is quite localized near the plate surface, even allowing for the increasing areas associated with the w_{diss} contours farther from the plate. It may be noted that the contours become almost spherical at 0·5 m from the centre of the plate, consistent with monopole-type radiation. The contours for the (1, 2) mode, in Figure 10(b), show an even more localized behaviour for w_{diss}, although this may be partly caused by increased propagation losses at this higher modal frequency (171·2 Hz, as opposed to

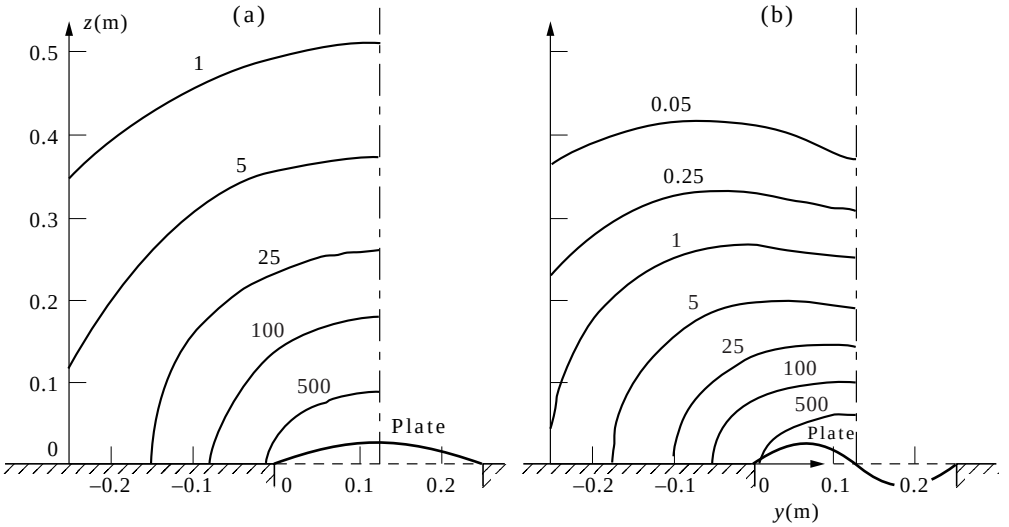

Figure 10. Sound power dissipation contours (in W/m^3) for $H = 0$: (a) the (1, 1) mode, (b) the (1, 2) mode.

51·7 Hz). Farther from the plate surface, the w_{diss} contours are characteristic of dipole radiation. Note that the typical "figure of eight" radiation pattern associated with the pressure far field of a dipole is not evident here, since—normal to the axis—there is still power dissipation *via* the (non-zero) velocity field, even though the sound pressure is zero.

It is of interest to see how the loss factor depends on the flow resistivity of the absorbent, as well as other parameters such as the width of the air gap. Some sample computed results—based on both damping models—are presented in Figures 11(a–d), for basalt wool, which is a commonly used sound-absorbing material. The range of σ is 1000–32 000 mks rayl/m in Figure 11(a) and 1000–128 000 mks rayl/m in Figures 11(b–d). In the case of the (1, 1) mode, predicted results from the coupled modal formulation are shown in Figure 11(a). For $\sigma > 32\,000$ mks rayl/m, it was not possible to obtain meaningful predictions because the peaks in $\Xi(\omega)$ (see equation (38)) were insufficiently well defined. It is observed that high degrees of damping can evidently be achieved for air spaces of 3 mm or less. For example, with an air gap of 2 mm and a flow resistivity of 32 000 mks rayl/m, a loss factor of about 1·4 is predicted. We can see that, for larger air gaps, the beneficial effect of high flow resistivity deteriorates as H increases. Computations for the loss factor of the (1, 1) mode based on the radiation model—and not shown here—indicate a progressive increase in η as σ increases, even for realistic air gaps. For example, for $H = 1$ mm and $\sigma = 128\,000$ mks rayl/m, a loss factor of four is forecast. It should be noted that, in the case of high flow resistivities (e.g., 128 000 mks rayl/m), frame motion in the absorbent could be significant in practice, causing small departures from the predicted damping.

Loss factor data for the (3, 1) mode, predicted from the radiation model, are shown in Figure 11(b). While the peak loss factor for $\sigma = 32\,000$ mks rayl/m is considerably lower here than it is for the (1, 1) mode, it is still about 0·6 for an air space of 0·4–0·8 mm, though it rapidly falls as H increases. For $\sigma = 128\,000$ mks rayl/m, η approaches 2 for very small air gaps. One can note that the loss factor for the higher flow resistivities actually falls below the curves for the lower flow resistivities as H increases beyond about 1 mm. It is likely that this effect occurs because the acoustic air flow partly by-passes the absorbent for large σ, and tends to "leak" across the air space between phase cells of opposite sign. Undulations in the loss factor curves—which were barely perceptible in the plots in Figure 11(a)—are now quite striking for H greater than about 10 mm. It is possible that the proposed leakage effect along the air gap might also be responsible for the fact that the loss factor curves in Figure 11(a), for large values of flow resistivity, approach one another for H greater than about 10 mm.

The loss factor for the (1, 2) and (2, 2) modes—again predicted by the radiation model—is shown in Figures 11(c, d). In the case of the (1, 2) mode (a volume-cancelling mode), the loss factor is generally lower than it is for the (3, 1) mode (a net volume-displacing mode), even though the frequency is higher. The loss factor figures for the (2, 2) mode are broadly similar to, though a little lower than, those for the (1, 2) mode.

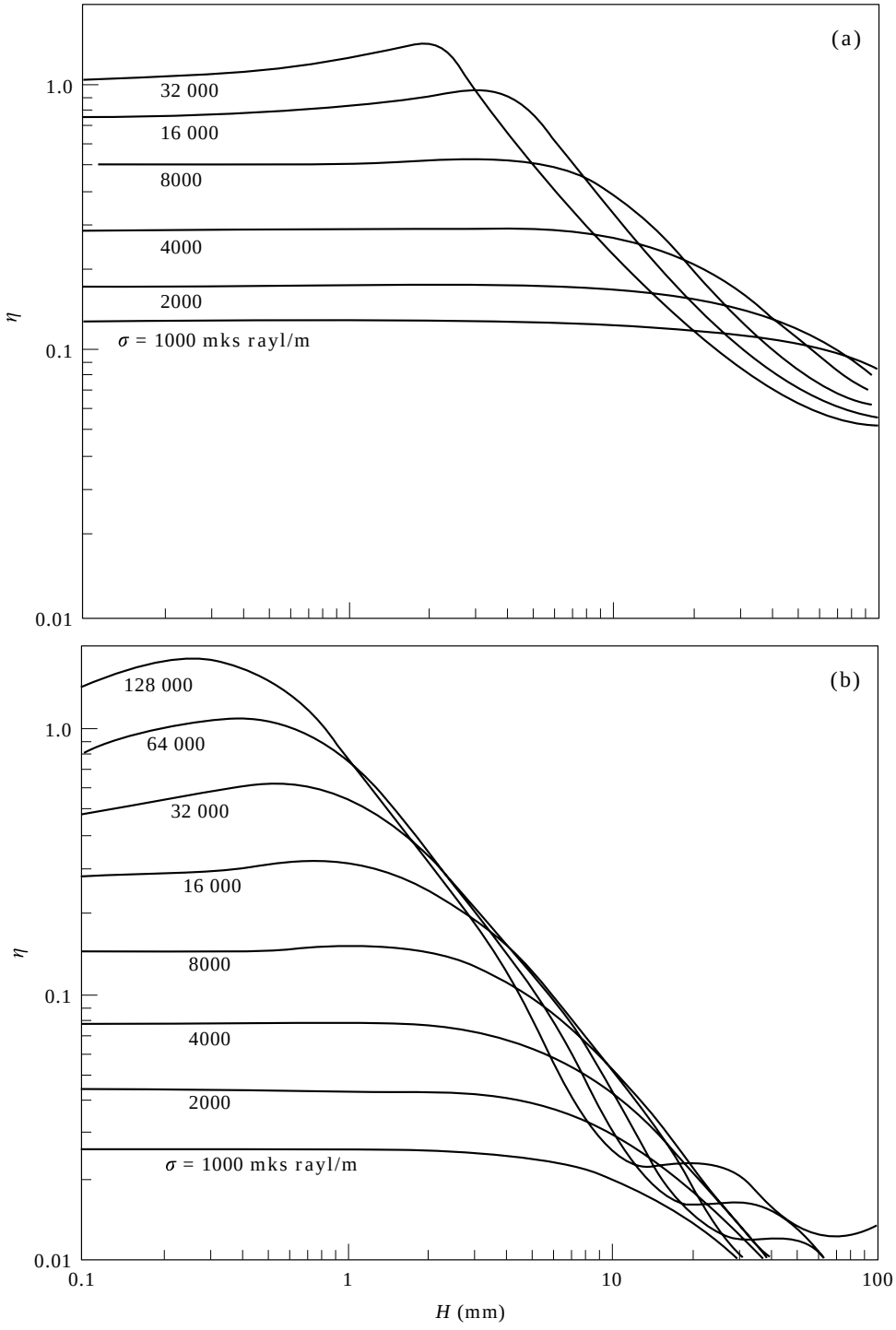

Figure 11. (a), (b) *Caption overleaf*.

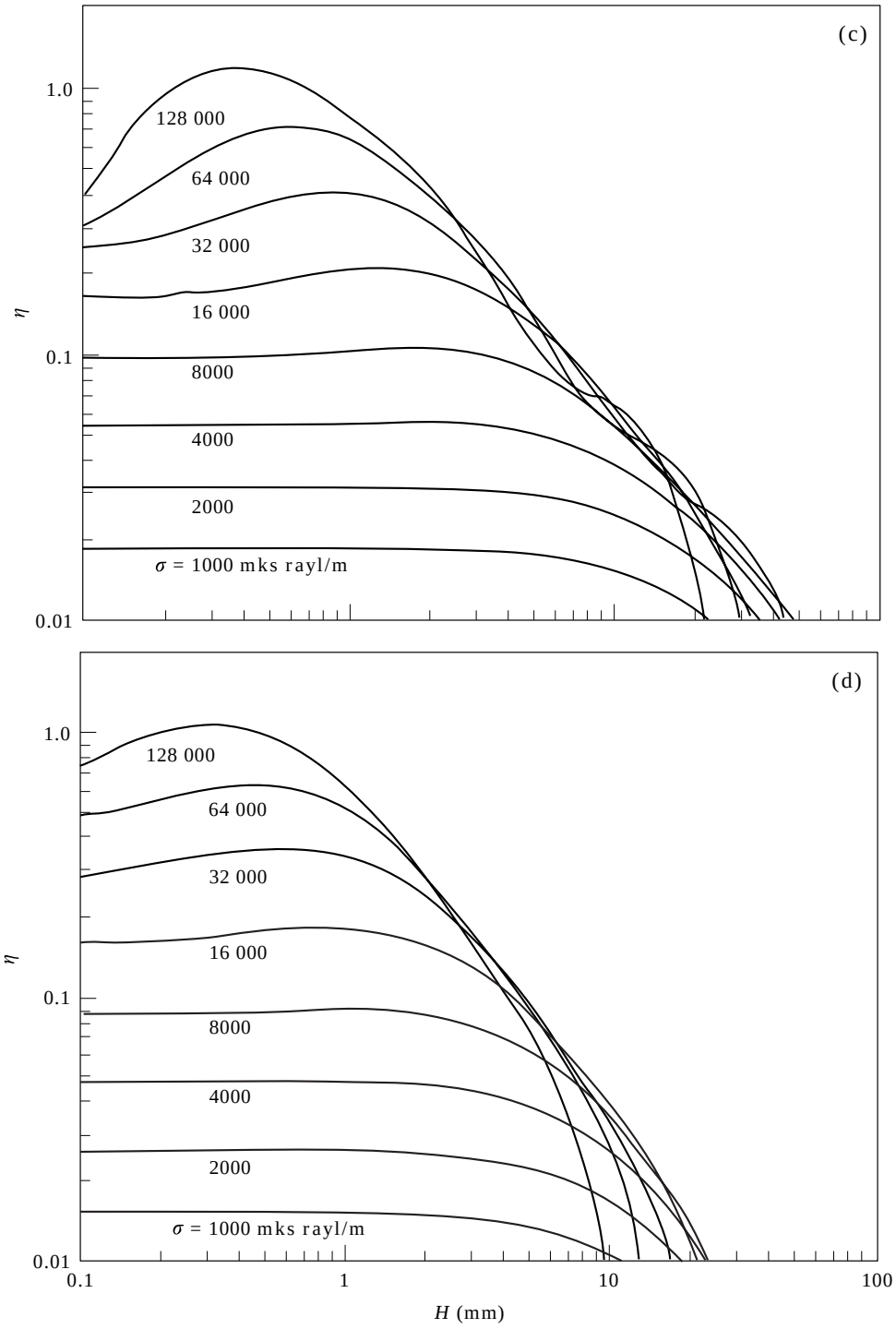

Figure 11. Predicted loss factor for the test plate with basalt wool absorbent, for a range of flow resistivities of the absorbent: (a) (1, 1) mode, (b) (3, 1) mode, (c) (1, 2) mode, (d) (2, 2) mode.

6. DISCUSSION AND CONCLUSIONS

The experimental data presented in this paper show that there is a dramatic increase in the damping of a flat plate brought about by the proximity of a porous sound absorbent. Very high levels of damping can be attained by this means, without the need for structural contact between the absorbent and the plate. The damping is quite strongly dependent on the mode of vibration of the plate, as would be expected.

The coupled modal formulation gives fairly good damping predictions for the (1, 1) mode but is less accurate for the higher modes, and the radiation model predicts the higher mode damping well but is inaccurate for the (1, 1) mode. The use of these two models in combination can therefore yield quite accurate predictions over the entire range of plate modes of interest.

Each of the two analytical models that have been described, for the prediction of damping, has its own virtues and drawbacks. The coupled modal analysis has the advantage of incorporating the effects a finite absorbent thickness and of taking into account the finite baffle dimensions. Its principal flaw relates to the assumption of a pressure release boundary condition at the edges of the absorbent layer and air gap, and at the walls of the duct into which sound emanating from the side of the absorbent layer remote from the plate is assumed to radiate. For the lowest few plate modes, the duct would present a purely reactive impedance to this radiation. Nonetheless, the numerical predictions of damping obtained from this model are in quite good agreement with measured data for the (1, 1) mode and in fair agreement for the (2, 1) mode. The radiation model does not, at present, include the effects of a finite absorbent thickness. This feature causes significant prediction error in the case of the (1, 1) plate mode, but is of minor consequence for the higher modes. The neglect of finite baffle dimensions in this model does not appear to be of great importance, at least in the case studied. The distribution of sound power dissipation per unit volume within the absorbent can be predicted by the use of this model, as can the intensity distribution over the plate surface.

The radiation model is capable of being extended to include the effects of a finite absorbent thickness, without excessive additional complication (the main extra effort appears to be in the evaluation of the Q functions—see equations (40a, b)—which becomes rather more tedious), and would be expected to yield a more accurate prediction of radiation from the (1, 1) plate mode. The coupled modal formulation has the potential for further refinement, though any very extensive modifications might detract from its present value as a computationally rapid tool that is suited for design optimization. More detailed analysis would probably be better done by the use of finite element techniques.

In both the theoretical models described here and in the experimental determination of its bulk properties, the absorbent was assumed to behave as an equivalent fluid with a rigid solid frame. While this assumption is usually well justified for absorbents of relatively low flow resistivity, it may not represent such a good approximation for very high values of σ. The scope of the present investigation did not permit a determination of the range of values of σ in which the equivalent fluid formulation is valid, for different materials. A separate study

would be required to provide such data, but to neglect frame motion seems a reasonable assumption for the great majority of common sound absorbing media.

The results presented here have relevance not only to structural damping in general, but also to damping mechanisms in the double-wall structure of an aircraft fuselage and to lightweight building partitions with absorbent in the air space, even though the physical system investigated here is considerably simpler. The near-field effect of the absorbent on the panel damping and the role of the air space between panel and absorbent are factors which will also play their parts in the vibrational interaction between each of the two leaves of a double wall and the absorbent placed between them. Of course, the lateral boundary conditions in a real double wall structure would normally be different from the pressure release condition assumed in the modal formulation and could introduce different effects. Rigid—rather than pressure release—boundaries might increase the damping further by causing a greater acoustic volume flow through the absorbent, for example. And in this case, the separation between plate and absorbent could be of lesser significance than that in the system examined here. At all events, the idealized physical system investigated here bridges the gap between the vibration of a simple panel and that of a full double-wall structure. It could also—if desired—be used to investigate the usefulness of a point-reacting representation of the absorbent, as opposed to the present bulk-reacting model, in a coupled modal analysis of a more complex system.

ACKNOWLEDGMENT

The work reported here was carried out with financial support from the European Commission, under BRITE/AERO Contract No. CT92 0032.

REFERENCES

1. R. J. Astley, A. Cummings and N. Sormaz 1991 *Journal of Sound and Vibration* **150**, 119–138. A finite element scheme for acoustic propagation in flexible-walled ducts with bulk-reacting liners, and comparison with experiment.
2. J. S. Bolton, N.-M. Shiau and Y. Kang 1996 *Journal of Sound and Vibration* **191**, 317–347. Sound transmission through multi-panel structures lined with elastic porous materials.
3. R. Panneton and N. Atalla 1996 *Journal of the Acoustical Society of America* **100**, 346–354. Numerical prediction of sound transmission through finite multilayer systems with poroelastic materials.
4. J.-F. Allard 1993 *Propagation of Sound in Porous Media*. Amsterdam: Elsevier Science.
5. M. E. Delany and E. N. Bazley 1970 *Applied Acoustics* **3**, 105–116. Acoustical properties of fibrous absorbent materials.
6. R. Kirby and A. Cummings *Proceedings of Euronoise* '95, *Lyon*, 21–23 *March* 1995, 835–840. Bulk acoustic properties of rigid fibrous absorbents extended to low frequencies.
7. K. Q. Xu 1997 *American Society of Mechanical Engineers Journal of Vibration and Acoustics* **119**, 265–270. Frequency domain modal parameter identification of high order systems in a numerically stable way.

8. W. M. Ewing, W. S. Jardetzky and F. Press 1957 *Elastic Waves in Layered Media*. New York: McGraw-Hill.
9. C. K. Amédin, A. Berry, Y. Champoux and J.-F. Allard 1995 *Journal of the Acoustical Society of America* **98**, 1757–1766. Sound field of a baffled piston source covered by a porous medium layer.
10. C. E. Wallace 1972 *Journal of the Acoustical Society of America* **51**, 946–952. Radiation resistance of a rectangular panel.